Journal of Inflammation Research

Dovepress
Taylor & Francis Group

Open Access Full Text Article

ORIGINAL RESEARCH

Electroacupuncture Regulates Oxidative Stress-Mediated NLRP3/ASC/Caspase-1 Pathway to Inhibit Microglial Activation: Alleviating Neuroinflammation and Depression in IBD

Zuqiang Li[1], Sihui Cao[1], Jingjing Yang[1], Lin Chen[1], Lv Jia[1], Penghui Lu[1], Jin Liu[2], Mi Liu[1], Qiong Liu[1]

[1]School of Acupuncture-Moxibustion, Tuina and Rehabilitation, Hunan University of Chinese Medicine, Changsha, Hunan, 410208, People's Republic of China; [2]Department of Psychiatry, National Clinical Research Center for Mental Disorders, and National Center for Mental Disorders, The Second Xiangya Hospital of Central South University, Changsha, Hunan, 410011, People's Republic of China

Correspondence: Mi Liu; Qiong Liu, School of Acupuncture-moxibustion, Tuina and Rehabilitation, Hunan University of Chinese Medicine, Changsha, Hunan, 410208, People's Republic of China, Email newmean@hnucm.edu.cn; 121181998@qq.com

Purpose: This study aims to investigate the efficacy of electroacupuncture in treating inflammatory bowel disease (IBD) accompanied by depressive symptoms. The potential mechanisms of electroacupuncture are also investigated, particularly in terms of its modulation of oxidative stress and NLRP3 inflammasomes to influence microglial activation and neuroinflammation, thereby alleviating depressive symptoms.

Material and methods: The inflammatory bowel disease model in mice was induced by dextran sulfate sodium (DSS), and the mice were randomly assigned to the CON group, DSS group, DSS+EA group, and DSS+ MCC950 group. The assessment of depressive-like behavior in mice involved behavioral tests, while the detection of oxidative stress in the PFC, NLRP3 inflammasomes, central inflammation expression, and microglial activation were conducted using enzyme-linked immunosorbent assay (ELISA), Western blot, immunofluorescence, and biochemical kits.

Results: Mice in the DSS group exhibited significant depressive-like behavior, which was effectively alleviated by electroacupuncture intervention. The intervention also reduced the expression of inflammatory factors and microglial activation in the medial prefrontal cortex (PFC) region. Electroacupuncture effectively attenuated oxidative stress, suppressed the recruitment of NLRP3 inflammasomes, and mitigated central nervous system inflammation, with effects similar to those of the NLRP3 inhibitor MCC950.

Conclusion: Electroacupuncture significantly alleviated depressive symptoms in IBD mice by inhibiting oxidative stress and microglial activation in the PFC region, thereby ameliorating the neuroinflammatory environment. The findings can provide new theoretical and scientific support for the clinical application of electroacupuncture in treating depressive symptoms associated with IBD.

Keywords: electroacupuncture, inflammatory bowel disease, depression symptoms, NLRP3, neuroinflammation

Introduction

Inflammatory Bowel Disease (IBD), including Crohn's Disease and Ulcerative Colitis, is a chronic condition characterized primarily by persistent intestinal inflammation.[1,2] Recent studies have demonstrated a higher prevalence of comorbid psychological or psychiatric disorders (particularly depressive symptoms) among patients with IBD, surpassing that observed in the general population.[3–5] The latest research suggests that neuroinflammation may play a critical role in depression symptoms induced by IBD.[6,7] The abnormal activation of microglial cells represents a central pathological feature of neuroinflammation.[8] Consequently, modulating the excessive activation of microglia and alleviating neuroinflammation are effective therapeutic strategies for managing comorbid IBD accompanied by depression.

Received: 14 April 2025
Accepted: 19 August 2025
Published: 29 August 2025

Neuroinflammation is closely associated with the abnormal activation of microglia, which serve as immune cells of the central nervous system responsible for dynamically maintaining the brain's internal environment. However, when peripheral inflammatory factors breach the blood-brain barrier and infiltrate into the brain, they stimulate the inflammatory activation of microglia, thereby inducing and exacerbating neuroinflammation.[9] Recent studies have shown that the NLRP3 inflammasome plays a pivotal role in mediating the inflammatory activation of microglia and can exacerbate the inflammatory response in the central nervous system.[10,11] The intensification of central neuroinflammation ultimately results in or intensifies depressive symptoms.[12,13] Moreover, oxidative stress has been found to impact the activation of the NLRP3 inflammasome.[14]

Electroacupuncture has been increasingly validated through clinical and animal studies as an effective intervention for treating IBD with comorbid depression. This traditional Chinese medicine approach is highly regarded for its potential to modulate immune responses and enhance neuroprotection. By activating specific biological pathways, electroacupuncture exhibits anti-inflammatory and neuroprotective properties, potentially contributing to its therapeutic effects on IBD and related depressive symptoms.[15,16] Clinical observations have revealed that an eight-week course of electroacupuncture can significantly alleviate the symptoms in patients with depression.[17] Moreover, animal studies have discovered that electroacupuncture can suppress microglia activation in the hippocampal and prefrontal cortical areas and modulate NLRP3 and NF-κB to relieve depressive symptoms in depression model animals.[18,19] Nevertheless, there is still a relative scarcity of studies investigating the specific mechanisms through which electroacupuncture mitigates depression symptoms caused by IBD.

Based on the previous findings, this study aims to explore the potential mechanisms of electroacupuncture in treating IBD-associated depression. Specifically, it focuses on how electroacupuncture regulates the oxidative stress-NLRP3/ASC/Caspase-1 pathway to inhibit abnormal microglial activation, reduce neuroinflammation, and alleviate depressive-like behaviors in mice with IBD-associated depression.

Materials and Methods

Experimental Animals

Male wild-type C57BL/6J mice at 6–8 weeks of age were provided by Slake Jingda Laboratory Animal Company Ltd (Hunan, China) and kept in the Animal Experiment Center of Hunan University of Traditional Chinese Medicine (License No.: SYXK [Xiang] 2019–0009). The mice were maintained under specific pathogen-free (SPF) conditions with a 12-hour light/12-hour dark cycle (lights on at 07:00) and housed in polypropylene cages with solid bottoms, accommodating 3–5 mice per cage and utilizing wood shavings as bedding. The room temperature was controlled at 22±1 °C, and the humidity was maintained at 60±10% throughout the experiment. Except for necessary experimental requirements, the mice had free access to food and water. The animal experiments in this study were approved and permitted by the Animal Experiment Ethics Committee of Hunan University of Traditional Chinese Medicine (LL-202209110002). All animals'protocols were strictly conducted following the Care and Use of Laboratory Animals by the National Academy of Sciences (8th edition).

Model Preparation and Intervention Methods

Ulcerative colitis was induced by administering a 2% aqueous solution of dextran sulfate (DSS) (MP Biomedicals, Cat# 9011–18-1) to the mice for seven consecutive days. The concentration and duration of DSS treatments were selected after calibration experiments with reference to a previous study.[20–23] The DSS solution was refreshed on a daily basis. During the administration period, the mice were closely monitored for general conditions and symptoms, including weight changes, stool consistency, and rectal bleeding. After a 7-day acclimation feeding period, the animals were randomly assigned into two groups based on their weight: control mice (CON group) and DSS-treated mice. The CON group was provided with tap water as their drinking source for one week, whereas the DSS group received a 2% DSS aqueous solution over the same period. Subsequently, further randomization was conducted within the DSS group, which was further divided into the DSS group, DSS+EA group, and DSS+MCC950 group. To induce sedation, mice were initially placed in an induction anesthesia chamber using a small animal respiratory anesthesia machine. Afterward, the mice were placed on a warming blanket and maintained under continuous anesthesia by securing their heads in a gas delivery mask. In the DSS+EA group, electroacupuncture was administered at specific acupoints, including Zusanli (ST36: located posterolateral to the knee joint, approximately 2 mm below the fibular head in mice), Tianshu (ST26: located 5 mm

lateral to the umbilicus), and Taichong (LR3: located between the first and second metatarsal bones on the dorsum of the foot). The EA intervention involved vertical insertion of acupuncture needles (13mm in length, 0.18mm in diameter; Huatuo, Suzhou Medical Supplies Co., Ltd.) at Zusanli and Tianshu acupoints to a depth of 2–5 mm below the skin and oblique insertion at Taichong to a depth of 1–2 mm. For the EA group, needling at Zusanli and Tianshu acupoints was alternated daily between the left and right sides, with intervention lasting for one week. Electro-stimulation was performed using a Korean-style electroacupuncture device (HANS-200, Nanjing Jisheng Medical Technology Co., Ltd)., delivering a current of 1 mA at a frequency of 2/15 Hz for 20 minutes. The EA treatment included inserting acupuncture needles (Huatuo, Suzhou Medical Supplies Factory Co., Ltd). measuring 13 mm in length and 0.18 mm in diameter into the unilateral Zusanli and Tianshu points, reaching a depth of 2–5 mm beneath the skin. In the DSS+EA group, the Zusanli and Tianshu points were alternately needled each day for a continuous intervention of 1 week. Mice in the DSS+MCC950 group received daily intraperitoneal injections of MCC950 (10 mg/kg) for two consecutive weeks. MCC950 is a potent and selective small-molecule inhibitor of the NLRP3 inflammasome. It was utilized in this study as a pharmacological positive control because it specifically blocks NLRP3-dependent ASC oligomerization and Caspase-1 activation, thereby inhibiting IL-1β and IL-18 processing and release. During the entire treatment process, the CON and DSS groups were only subjected to routine anesthesia and restraint. The preparation of the IBD mouse model and the treatment process are illustrated in Figure 1A.

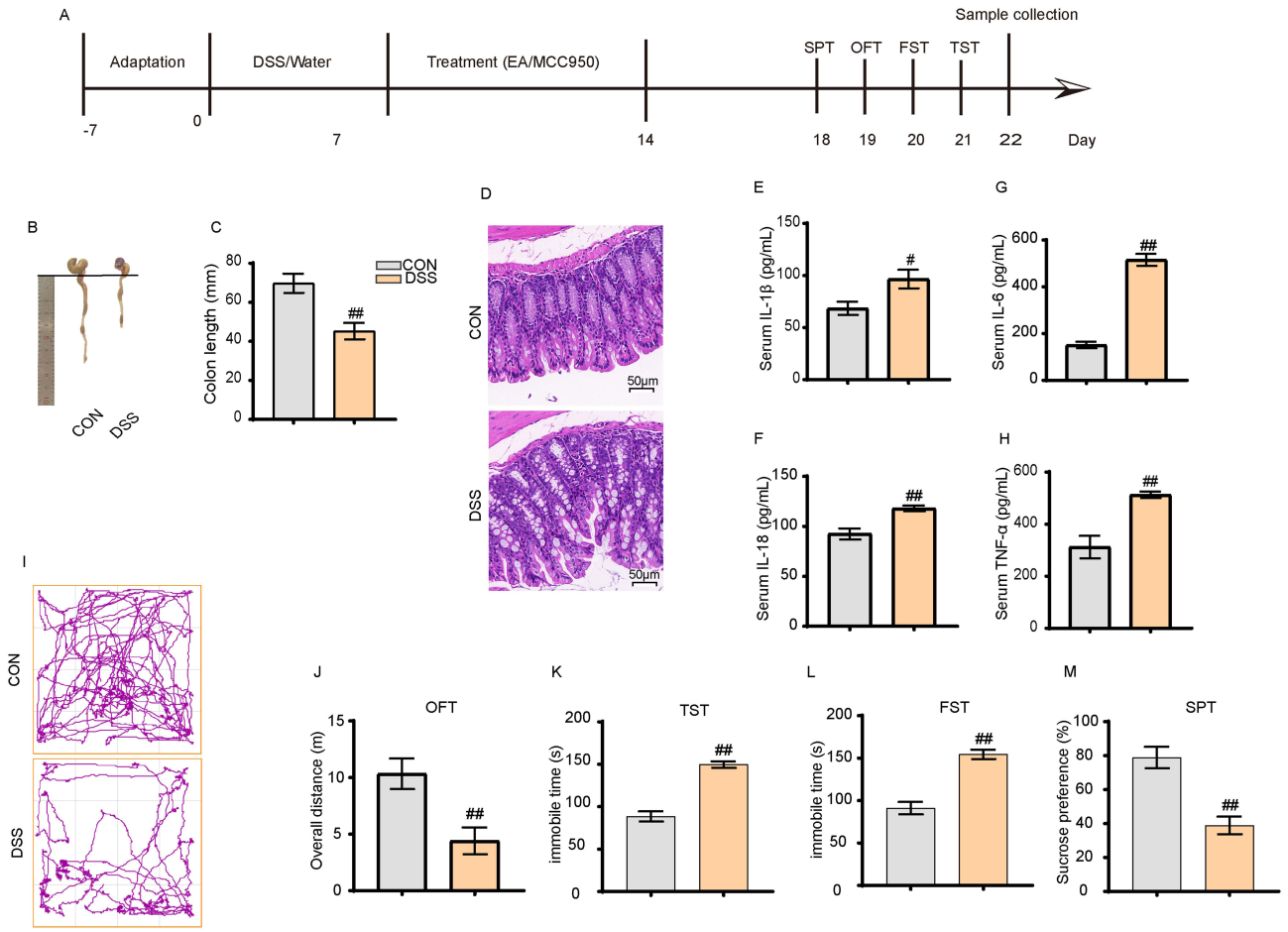

Figure 1 2% DSS induced inflammatory bowel disease with depressive-like symptoms in mice. (**A**) Overall experimental timeline. (**B** and **C**) DSS treatment resulted in significant shortening of the colon in mice. (**D**) DSS induced colonic inflammation (40×). (**E**–**H**) DSS increased the levels of peripheral inflammatory cytokines IL-1β, IL-6, IL-8, and TNF-α. (**I** and **J**) Representative movement tracks and total distance traveled over 4 minutes in the open field test. (**K**–**M**) DSS prolonged immobility time in the TST and FST, and reduced sucrose intake. All data are presented as mean ± standard error of the mean, #p<0.05, ##p<0.01 compared to the control group. (n=10 per group).
Abbreviations: OFT, Open Field Test; TST, Tail Suspension Test; FST, Forced Swim Test; SPT, Sucrose Preference Test.

https://doi.org/10.2147/JIR.S534219

Sample Collection and Processing

Tissue sampling was conducted after completing the treatment and behavioral assessments. Anesthesia was initially induced by injecting 0.6 mL of a 1.5% sodium pentobarbital solution. Subsequently, mice requiring immunofluorescence staining of brain sections underwent cardiac perfusion with 0.9% saline solution, followed by extraction of the entire brain, preservation in 4% paraformaldehyde, and storage at 4°C. For mice designated for ELISA, Western Blot (WB), q-PCR, and biochemical assays of the PFC area, euthanasia was performed via decapitation. The PFC was subsequently dissected and stored at −80°C. Blood samples were collected from mice through ocular bleeding, and serum was separated using high-speed centrifugation. Finally, the separated serum was preserved in a −80°C freezer for a subsequent experiment.

Assessment of Depression-Like Behaviors

The mice were acclimated to the testing environment for at least 24 hours for all behavioral tests and underwent minimal handling in a completely quiet setting. The tests were separated by at least one day for proper rest intervals. Following each assessment, all chambers were thoroughly sanitized with 75% ethanol to eliminate potential olfactory cues in the equipment. The mice's behavior was recorded using the ANY-maze video tracking system and subsequently analyzed offline. The observers remained blinded to the experimental objectives.

Open Field Test (OFT)

This test was conducted in a dimly illuminated room. The mouse was positioned within one corner of a square enclosure constructed from white wooden boards (50×50 cm^2), surrounded by white wooden boards (50 cm high). The mouse was allowed to explore its surroundings for 5 minutes freely, and its movement distance was recorded.

Sucrose Preference Test (SPT)

The mice were housed individually and provided with two identical bottles of tap water on the first day, which were replaced by two bottles of 1% sucrose solution on the second day. On the third day, the mice were water-deprived for 24 hours. Subsequently, the mice were provided with two bottles, one filled with 1% sucrose solution and the other with tap water. The sucrose solution bottle was randomly placed on the left or right side of the cage to avoid side preferences. Finally, the intake of each type of liquid was quantified, and the sucrose preference rate was determined by calculating the weight change of the sucrose solution relative to the total weight change of both bottles.

Tail Suspension Test (TST)

The mouse was individually suspended by taping its tail vertically about 1 cm from its tip, approximately 50 cm above the floor. During the 6-minute test, a blinded observer measured the duration of immobility time in the last 4 minutes.

Forced Swimming Test (FST)

Each mouse was gently immersed in a transparent plastic cylinder with a diameter of 15 cm and a height of 35 cm filled with water at a temperature of 20±1°C (the mouse did not contact the cylinder bottom while swimming). During the 6-minute test, an initial 2-minute adaptation period was conducted, followed by the observer's documentation of immobility duration over the subsequent 4 minutes. Immobility was defined as the absence of active escape-oriented behaviors, characterized by maintaining a fixed posture in one place or minimizing paw movements to keep the head above water. Prolonged immobility was considered "behavioral despair".

Enzyme-Linked Immunosorbent Assay (ELISA)

The serum and brain tissues were homogenized and centrifuged to detect pro-inflammatory factors. According to the manufacturer's protocol, the protein levels of IL-6 (LMB, Cat# LM-IL-6), IL-18 (LMB, Cat# LM-IL-18β), TNF-α (LMB, Cat# LM-TNF-α), and IL-1β (LMB, Cat# LM-IL-1β) were analyzed using corresponding ELISA kits. The absorbance was measured at a wavelength of 450 nm.

Western Blot (WB)

Total proteins were extracted from brain tissue or cells using lysates containing RIPA buffer supplements, protease inhibitors, and phosphatase inhibitors. The protein concentration of each sample was determined using the bicinchoninic acid (BCA) assay (Biotinyan, Shanghai). Subsequently, proteins were separated using SDS-PAGE gel electrophoresis and transferred onto a polyvinylidene fluoride (PVDF) membrane (Millipore, USA). Following a 5% milk or BSA blocking step, the membranes were incubated overnight at 4°C with the primary antibodies as follows: NF-κB (ProteinTech, Cat#10745-1-AP, 1:2000); p-NF-κB (ProteinTech, Cat#82335-1-RR, 1:3000); NLRP3 (ProteinTech, Cat#19771-1-AP, 1:1200); ASC (ProteinTech, Cat#10500-1-AP, 1:4000); Caspase-1 (ProteinTech, Cat#22915-1-AP, 1:2000); GSDMD (ProteinTech, Cat#20770-1-AP, 1:1000); GSDMD-N (Affinity, Cat# DF13758, 1:1000); β-actin (ProteinTech, Cat#66009-1-lg, 1:5000). After performing three washes with TBST buffer (10 minutes each), the membranes were incubated with secondary rabbit or anti-mouse antibodies at room temperature for 1 hour. Enhanced chemiluminescence was employed to visualize the protein bands, and data analysis was performed using ImageJ software (NIH, USA).

Immunofluorescence

Brain sections with a thickness of 30 μm were dewaxed using a stepwise ethanol-to-water gradient. Next, antigen retrieval was performed on the slices using citrate buffer (pH 6.0), followed by blocking with a 3% hydrogen peroxide solution. The sections were washed with phosphate-buffered saline (PBS) and subsequently blocked with serum for further experiments. The tissue was incubated overnight at 4°C with an anti-Iba1 (1:200) secondary antibody. After completing these procedures, the slices were rinsed with PBS and incubated with HRP-labeled secondary antibody at room temperature for 1 hour. Subsequently, the sections were washed again with PBS before being treated with tyramide signal amplification (TSA) reagent (1:1000) at 37 °C for 30 minutes. These steps were repeated for double staining using the anti-NLRP3 (ProteinTech, Cat#10745-1-AP) antibody. Finally, an anti-fade sealer was added, and the slides were encapsulated upon completion of the PBS wash and DAPI staining of the samples. An inverted fluorescence microscope (Zeiss, Germany) was employed to capture images for the quantitative analysis with Image J.

HPLC (High-Performance Liquid Chromatography) Analysis

Briefly, 0.06 g of the sample (accurate to 0.0001 g) was weighed and placed in a 1.5 mL transparent centrifuge tube, and 1 mL of methanol was added. The mixture was homogenized and vortexed for 1 min to ensure thorough mixing. Then, the mixture was sonicated at a low temperature for 30 min. After sonication, the mixture was centrifuged at 4000 rpm for 10 min, and the supernatant was transferred to a new centrifuge tube. This process was repeated twice, and all three supernatant fractions were combined and evaporated under nitrogen at room temperature until the volume reached 0.5 mL. Subsequently, the supernatant was passed through a 0.22 μm filter before quantifying 4-HNE using high-performance liquid chromatography (HPLC1100) with electrochemical detection. The mobile phase consisted of water (A) and methanol (B), and the flow rate was 1 mL/min. The 4-HNE was separated using a cation-exchange guard column (1.0 mm I.D. × 15 mm) followed by a protected cation-exchange column (2.0 mm I.D. × 200 mm). Electrochemical detection was conducted using an electrochemical detector (ECD-700, Eicom, Kyoto, Japan) with a glass working electrode at a potential of +50 mV.

Tissue Biochemical Index Assay

The samples were analyzed using commercial assay kits for glutathione peroxidase (GPx) activity (LBM, LMB-W-A202) and protein carbonyl content (LBM, LMB-W-A405), according to the manufacturer's instructions. Specifically, GPx activity and protein carbonyl content were measured after extraction according to the manufacturer's procedures, and the absorbance was determined at wavelengths of 340 nm and 370 nm using a microplate reader.

Quantitative-Polymerase Chain Reaction (q-PCR)

Total RNA was isolated from the mouse PFC samples using the Total RNA Isolation Kit (Vazyme, RC101-01). cDNA synthesis was performed with HiScript II Q RT SuperMix (Vazyme, R223-01). The SYBR Green-based real-time

Table 1 Primer Sequences Used in Real-Time RT-PCR Analysis

Gene		Sequence	Product
Mus_GAPDH	Forward	GCCTCCTCCAATTCAACCCT	145 bp
	Reverse	CCCAATACGGCCAAATCCGT	
Mus_NLRP3	Forward	CCTTAAGCTGGAGCTGCTGT	188 bp
	Reverse	TCACCTCTCGGCAGTGGATA	
Mus_Caspase 1	Forward	TGCCTGGTCTTGTGACTTGG	100 bp
	Reverse	GGTCACCCTATCAGCAGTGG	
Mus_ASC	Forward	TGAGCAGCTGCAAACGACTA	200 bp
	Reverse	CACGAACTGCCTGGTACTGT	
Mus_GSDMD	Forward	GATCAAGGAGGTAAGCGGCA	195 bp
	Reverse	CACTCCGGTTCTGGTTCTGG	
Mus_NF-κB	Forward	GGCTACACAGGACCAGGAAC	154 bp
	Reverse	CTCTATAGGAACTATGGATACTGCG	

quantitative PCR method was utilized, and the gene expressions of NLRP3, ASC, Caspase-1, GSDMD, and NF-κB were determined on a fluorescence quantitative PCR instrument (Keopu Medical), with GAPDH as the internal reference gene. The primer sequences are presented in Table 1. The PCR conditions were initial denaturation at 95°C for 30s, followed by 40 cycles with denaturation at 95°C for 10s and annealing at 65°C for 30s. The relative gene expression levels were determined using the $2^{-\Delta\Delta Ct}$ method.

H&E (Hematoxylin-Eosin) Staining

Colon tissue samples collected from the mice were dehydrated using sequential ethanol solutions (70%, 80%, and 90%). The samples were then immersed in a 1:1 mixture of pure ethanol and xylene for 15 min. After that, the samples were treated with xylene I for 15 min and xylene II for another 15 min until transparency was achieved. After that, the samples were placed in a 1:1 mixture of paraffin and xylene for 15 min. Subsequently, they were transferred to paraffin I and paraffin II for wax infiltration for 50 to 60 min. Following that, the samples were embedded in paraffin and sectioned. After baking, the paraffin sections were dewaxed and rehydrated before staining them with hematoxylin solution for 3 min and differentiating them using hydrochloric acid ethanol solution for 15s. After briefly rinsing with water and treating with the bluing reagent for 15s, the sections were rinsed under running water. Eosin staining was carried out for 3 min, followed by rinsing under running water, dehydration, and mounting. Finally, the histological changes in the colon were observed.

Statistical Analysis

The experimental data are expressed as mean ± standard deviation. A two-tailed unpaired Student's *t*-test was performed to compare two independent samples. In the case of a two-factor design with a single independent variable or a two-way ANOVA when comparing more than two groups, a one-way ANOVA was performed, followed by Bonferroni's post hoc test to further examine pairwise group differences. All statistical analyses and graphical representations were conducted in GraphPad Prism 8 (GraphPad Software, Inc., USA). Significance levels are indicated as follows: * (#) indicates $P < 0.05$, and ** (##) indicates $P < 0.01$. $P < 0.05$ was considered statistically significant.

Results

IBD Mice Display Pronounced Depression-Like Behaviors

As shown in Figure 1, the mouse colons in the DSS group were significantly shorter than the CON group ($p < 0.01$) (Figure 1B and C). H&E staining revealed significant inflammatory infiltration, nuclear pyknosis, and cell membrane swelling in the colons of the DSS group (Figure 1D). ELISA results indicated significantly higher expression levels of inflammatory markers IL-1β and TNF-α in the serum of the DSS group than in the CON group ($p < 0.01$) (Figure 1E–H). These results indicate that the 2% DSS successfully induced IBD mouse models. Subsequent behavioral tests were conducted to assess whether IBD mice exhibited depressive symptoms, including open field tests, tail suspension tests, forced swim tests, and sucrose preference tests. The results showed that, compared to the CON group, the DSS group had a significantly reduced movement distance in the open field tests (Figure 1I and J), increased immobility time in the tail suspension and forced swim tests (Figure 1K and L), and a markedly decreased sucrose preference rate ($p < 0.01$) (Figure 1M). These results demonstrate that the IBD mouse models induced by the 2% DSS exhibited depressive-like behaviors.

Significant Neuroinflammation Is Observed in the PFC Region of IBD Mice

ELISA analysis of the PFC brain region revealed significantly higher expression levels of inflammatory factors IL-1β, IL-6, IL-18 and TNF-α in the DSS group compared to the CON group ($p < 0.01$) (Figure 2A–D). Western Blot analysis demonstrated that the DSS group had significantly increased levels of nuclear transcription factor NF-κB p65 and its phosphorylated form p-NF-κB p65 compared to the CON group ($p < 0.01$) (Figure 2E–G). q-PCR analysis was conducted to further investigate NF-κB expression, which found significantly higher mRNA transcription levels of NF-κB in the DSS group ($p < 0.01$) (Figure 2H).

Electroacupuncture Alleviates Inflammatory Levels in the Intestine and PFC of IBD Mice and Reduces Depression-Like Behaviors

The H&E staining results of the colon revealed that, compared to the DSS group, the DSS+EA group exhibited a more organized colon epithelial cell arrangement, decreased inflammatory infiltration, and smoother cell membranes

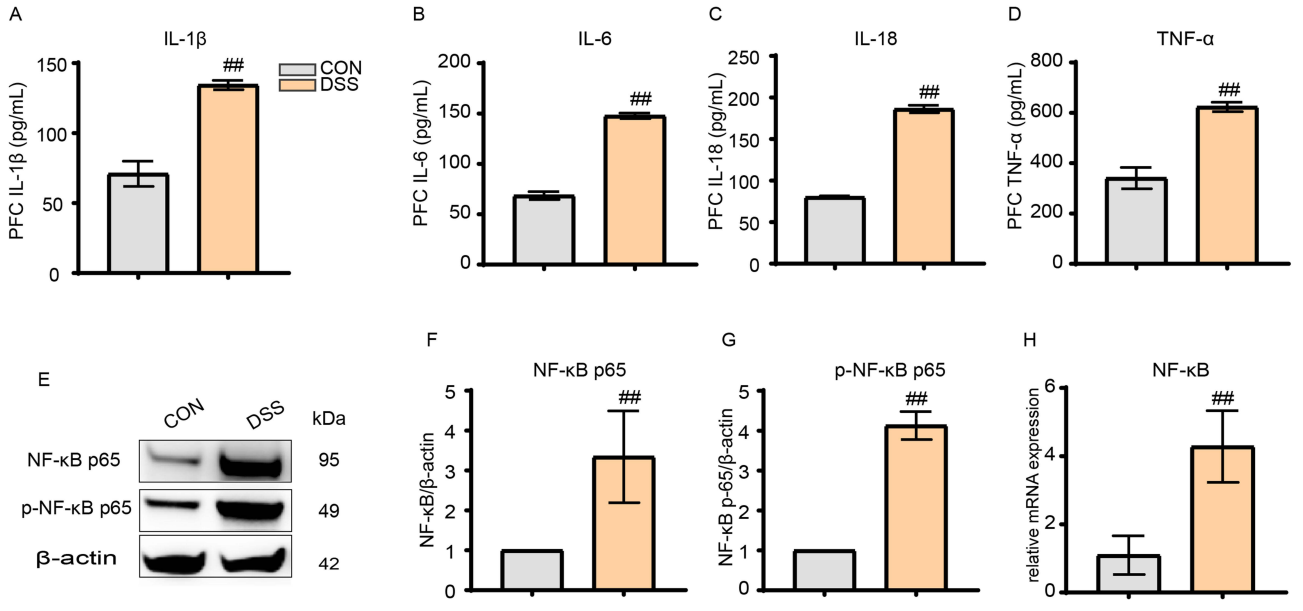

Figure 2 DSS induced neuroinflammation in mice. (**A–D**) DSS modeling increased the levels of IL-1β, IL-6, IL-18, and TNF-α in the PFC region. (**E–G**) DSS treatment resulted in elevated relative expression of NF-κB p65 and p-NF-κB p65. (**H**) DSS caused increased mRNA transcription of NF-κB in the PFC region. All data are presented as mean ± standard error of the mean, ##p<0.01 compared to the control group. (n=10 per group).

Abbreviations: IL-1β, Interleukin-1 beta; IL-6, Interleukin-6; IL-18, Interleukin-18; TNF-α, Tumor Necrosis Factor-alpha; NF-κB p65, Nuclear Factor kappa-light-chain-enhancer of activated B cells p65 subunit; p-NF-κB p65, phosphorylated NF-κB p65; PFC, Prefrontal Cortex.

https://doi.org/10.2147/JIR.S534219

(Figure 3A). Additionally, the ELISA findings showed that following electroacupuncture treatment, the inflammatory cytokines IL-1β, IL-6, IL-18 and TNF-α decreased markedly in the DSS+EA group ($p < 0.01$) (Figure 3B–E). Intestinal inflammation decreased noticeably. WB analysis of the PFC indicated that the DSS+EA group had significantly reduced levels of nuclear transcription factor NF-κB p65 and its phosphorylated p-NF-κB p65 than the DSS group ($p < 0.01$) (Figure 3F–H). Likewise, the NF-κB mRNA transcription levels in the DSS+EA group were markedly reduced compared to the DSS group ($p < 0.05$) (Figure 3I). After electroacupuncture treatment, the depressive-like behaviors decreased significantly. Specifically, the DSS+EA group showed a significantly longer movement distance than the DSS group in the open field tests ($p < 0.01$) (Figure 3J and K), significantly reduced immobility time in the open field and forced swim tests ($p < 0.01$) (Figure 3L and M), and a significantly increased sucrose preference rate (SPR) ($p < 0.01$) (Figure 3N).

Electroacupuncture Alleviates Inflammation in the PFC of IBD Mice by Inhibiting Excessive Microglial Activation

Immunofluorescence (IF) findings indicated that the DSS group had more Iba1-positive cells than the CON group ($p < 0.01$). Following electroacupuncture treatment, the DSS+EA group showed markedly reduced Iba1-positive cells relative

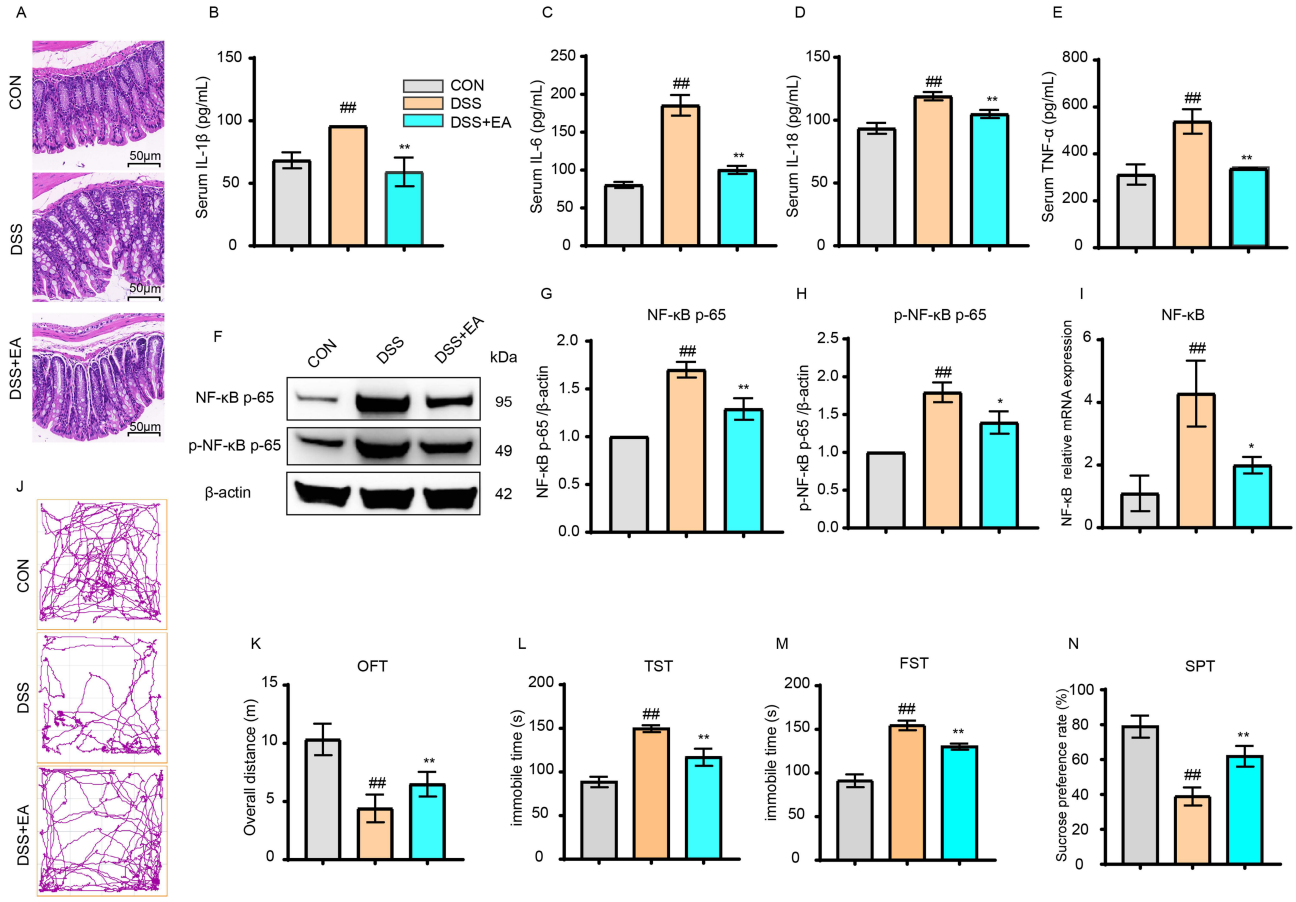

Figure 3 Electroacupuncture alleviated DSS-induced colonic and central inflammation, as well as depressive-like symptoms (40×). (**A**) Electroacupuncture (EA) improved intestinal morphology in IBD mice. (**B**–**E**) EA reduced the expression levels of IL-1β, IL-6, IL-18, and TNF-α in the intestines of IBD mice. (**F**–**H**) EA decreased the protein expression of NF-κB p65 and p-NF-κB p65 in the PFC region. (**I**) EA reduced the mRNA transcription of NF-κB in the PFC region. (**J** and **K**) EA increased the total distance traveled by IBD mice in the open field test (OFT). (**L**–**N**) EA decreased immobility time in the tail suspension test (TST) and forced swim test (FST), and increased sucrose intake. All data are presented as mean ± standard error of the mean, ##p<0.01 compared to the CON group. *p<0.05, **p<0.01 compared to the DSS group. (n=10 per group).

Abbreviations: IL-1β, Interleukin-1 beta; IL-6, Interleukin-6; IL-18, Interleukin-18; TNF-α, Tumor Necrosis Factor-alpha; NF-κB p65, Nuclear Factor kappa-light-chain-enhancer of activated B cells p65 subunit; p-NF-κB p65, phosphorylated NF-κB p65; q-PCR, quantitative Polymerase Chain Reaction; PFC, Prefrontal Cortex; IBD, Inflammatory Bowel Disease; OFT, Open Field Test; TST, Tail Suspension Test; FST, Forced Swim Test; SPT, Sucrose Preference Test.

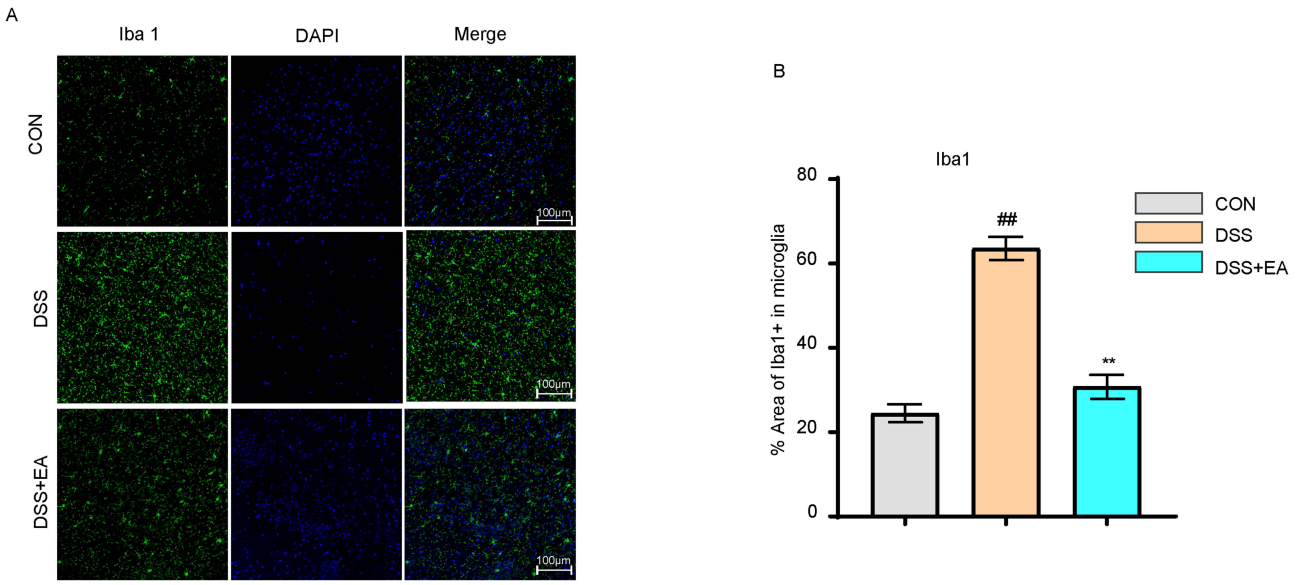

Figure 4 Electroacupuncture inhibited microglial activation in the PFC of IBD mice. (**A**) Representative images of Iba1+ immunofluorescence in the PFC (40× magnification). (**B**) Electroacupuncture reduced the expression of $Iba1^{+}$. All data are presented as mean ± standard error of the mean, ##p<0.01 compared to the CON group**p<0.01 compared to the DSS group. (n=10 per group).
Abbreviations: Iba1, Ionized calcium-binding adapter molecule 1; DAPI, 4′,6-Diamidino-2-phenylindole.

to the DSS group ($p < 0.01$) (Figure 4A and B). These results indicate that electroacupuncture inhibits microglial cell activation.

Electroacupuncture Suppresses Microglia Overactivation by Modulating the NLRP3/ASC/Caspase-1 Pathway

IF results showed that the number of NLRP3-positive cells was significantly higher in the DSS group than the CON group ($p < 0.01$) but significantly lower in the DSS+MCC950 group compared to the DSS group ($p < 0.01$) (Figure 5A and B). Similarly, the DSS+EA group also showed a significantly decreased number of NLRP3-positive cells than the DSS group ($p < 0.01$) (Figure 5A and B). The positive expression of Iba1 in the PFC is similar to that of NLRP3. Compared with the CON group, the positive expression of Iba1 in the DSS group was significantly increased ($p < 0.01$), but the expression of Iba1 in the DSS+MCC950 group was significantly decreased ($p < 0.01$). At the same time, the results of the DSS+EA group were similar to those of the DSS+MCC950 group, and the positive expression of Iba1 was significantly lower than that of the DSS group ($p < 0.01$) (Figure 5C). In order to further investigate the regulatory effect of electroacupuncture on NLRP3, Western Blot analyses were performed on the signaling pathways associated with the NLRP3 inflammasome. The results revealed that, compared to the DSS group, the relative expression levels of NLRP3, ASC, Caspase-1, GSDMD, and GSDMD-N in the DSS+EA and DSS+MCC950 groups were significantly reduced ($p < 0.01$) (Figure 5D–I).

Electroacupuncture Decreases NLRP3 Inflammasome Recruitment by Suppressing Oxidative Stress within Microglia

GPx, Protein Carbonyl, and 4-HNE are crucial indicators of oxidative and antioxidative processes during oxidative stress. The biochemical data indicated significantly elevated levels of antioxidant enzyme GPx in the DSS+EA and DSS +MCC950 groups compared to the DSS group ($p < 0.01$) (Figure 6A), whereas Protein Carbonyl levels were markedly reduced relative to the DSS group ($p < 0.01$) (Figure 6B). LC-MS analysis revealed that the 4-HNE contents in the DSS +EA and DSS+MCC950 groups were significantly lower than in the DSS group ($p < 0.01$) (Figure 6C). These results indicate that electroacupuncture can significantly inhibit oxidative stress. To clarify the relationship between oxidative stress and NLRP3, q-PCR tests were conducted on NLRP3, ASC, and Caspase-1. The results showed significantly lower

https://doi.org/10.2147/JIR.S534219

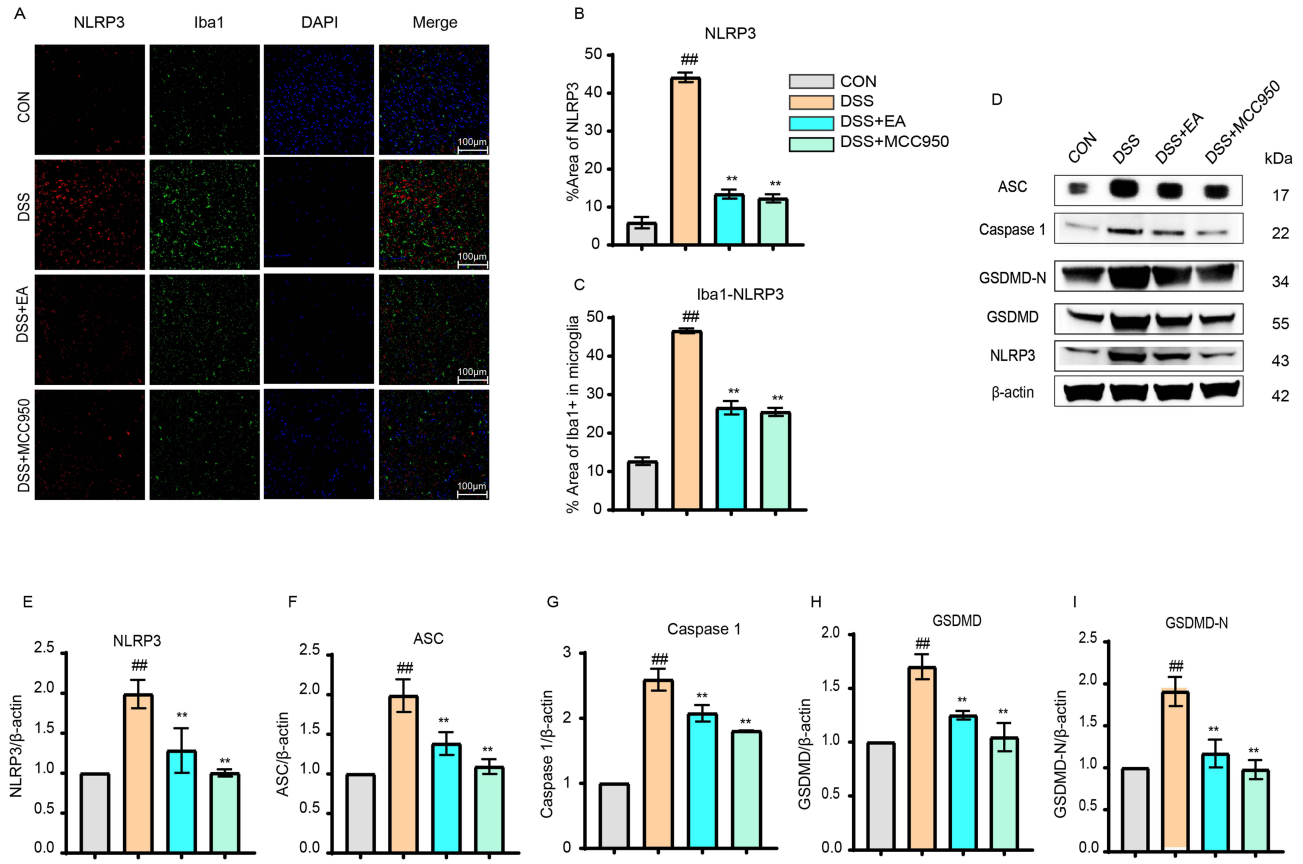

Figure 5 Electroacupuncture regulated the NLRP3/ASC/Caspase 1/GSDMD pathway. (**A**) Representative immunofluorescence images of NLRP3 and Iba1+ expression in the PFC (40× magnification). (**B**) Electroacupuncture (EA) reduced the number of NLRP3+ cells. (**C**) EA reduced the expression of Iba1+ marker. (**D–I**) EA decreased the relative protein expression levels of NLRP3, ASC, Caspase 1, GSDMD, and GSDMD-N in the PFC region. All data are presented as mean ± standard error of the mean, ##p<0.01 compared to the CON group. **p<0.01 compared to the DSS group. (n=10 per group).

Abbreviations: NLRP3, NOD-like receptor family pyrin domain containing 3; ASC, Apoptosis-associated speck-like protein containing a CARD; Caspase-1, Cysteine-aspartic protease-1; GSDMD, Gasdermin D; GSDMD-N, N-terminal fragment of Gasdermin D; Iba1, Ionized calcium-binding adapter molecule 1; DAPI, 4′,6-Diamidino-2-phenylindole; MCC950, NLRP3-selective inhibitor.

mRNA transcription levels of NLRP3, ASC, and Caspase-1 in the DSS+EA and DSS+MCC950 groups than the DSS group ($p < 0.01$) (Figure 6D–G).

Discussion

Recently, the comorbidity of IBD complicated with psychiatric disorders, particularly anxiety and depression, has garnered extensive academic attention.[24] Neuroinflammation was identified as a crucial pathological mechanism underlying the comorbidity of IBD complicated with depression.[25] This study found that IBD mouse models induced by DSS exhibited significant depressive-like behaviors, accompanied by abnormal microglial activation and neuroinflammatory changes in PFC. After electroacupuncture intervention, the IBD models exhibited fewer depressive-like behaviors, lower abnormal microglial activation, and alleviated neuroinflammation. Thus, the NLRP3/ASC/Caspase-1 signaling pathway mediated by oxidative stress plays a crucial role in these effects.

As a chronic systemic inflammatory disease, IBD induces localized inflammatory responses in the intestines and releases substantial pro-inflammatory cytokines (eg, TNF-α, IL-6, and IL-1β) into the bloodstream. These cytokines can cross the blood-brain barrier or transmit to the central nervous system via the vagus nerve, thereby inducing neuroinflammation in the brain.[26,27] As the most widespread immune cells in the brain, microglia play crucial roles in immune defense, waste clearance, neural environment stability, and neural repair and disease processes.[28,29] Persistent inflammatory stimuli lead to abnormal microglial cell activation, inducing them to adopt a pro-inflammatory phenotype. As a

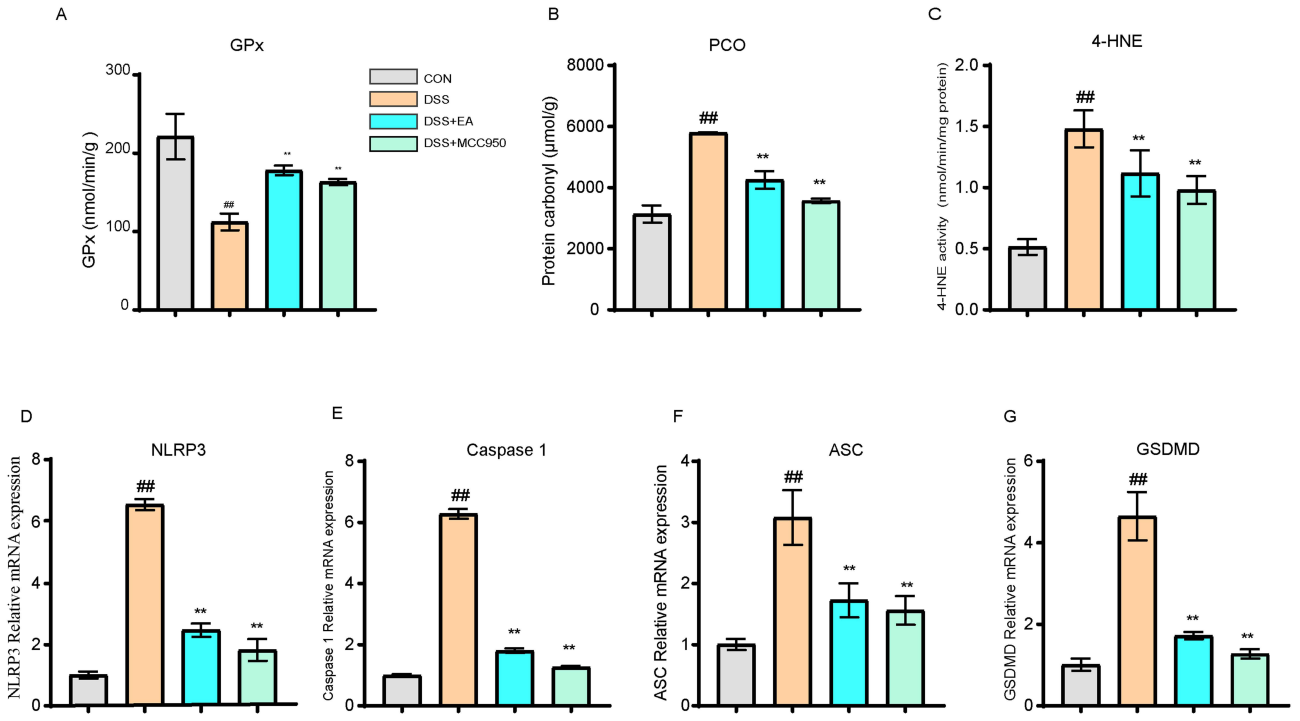

Figure 6 Electroacupuncture reduces NLRP3 activation by inhibiting oxidative stress. (**A**) Electroacupuncture (EA) increased the expression of GPx in the PFC region. (**B**) EA reduced the expression of protein carbonyls. (**C**) EA decreased the protein level of 4-HNE in the PFC region. (**D**–**G**) EA reduced the mRNA transcription of NLRP3, ASC, Caspase 1, and GSDMD in the PFC region. All data are presented as mean ± standard error of the mean, ##p<0.01 compared to the CON group. **p<0.01 compared to the DSS group. (n=10 per group).

Abbreviations: GPx, Glutathione Peroxidase; PCO, Protein Carbonyl; 4-HNE, 4-Hydroxynonenal; MCC950, NLRP3-selective inhibitor; NLRP3, NOD-like receptor family pyrin domain containing 3; ASC, Apoptosis-associated speck-like protein containing a CARD; Caspase-1, Cysteine-aspartic protease-1; GSDMD, Gasdermin D.

result, substantial pro-inflammatory cytokines are released, which disrupt the normal functionality and structural integrity of neurons, compromise neural plasticity, and ultimately trigger depressive symptoms.[8,30,31] Numerous studies indicated that the pathophysiological progression of depression is companied by abnormal microglial cell activation in various brain regions, such as the prefrontal cortex, hippocampus, and anterior cingulate cortex.[32–35] Consequently, the primary clinical treatment strategies for IBD with comorbid depression involve inhibiting the abnormal microglial cell activation and alleviating neuroinflammation.

Clinically, IBD treatments mainly involve managing intestinal inflammation and addressing co-occurring depressive symptoms. Numerous therapeutic approaches mitigate inflammation by suppressing inflammatory cytokines. Biological agents like the anti-TNF medications infliximab (IFX) and adalimumab (ADA) effectively relieve IBD symptoms and depression by inhibiting specific cytokines.[36–38] The JAK inhibitor tofacitinib (TOFA) disrupts the JAK-STAT signaling pathway, reduces inflammatory responses, and alleviates depressive symptoms in IBD.[39] Additionally, therapies modulating the gut microbiota, such as probiotics, reduce inflammation by influencing the gut-brain axis, thereby alleviating depressive symptoms.[40,41] This study found that electroacupuncture alleviated IBD symptoms and significantly mitigated depression by modulating the neuroimmune system and reducing inflammatory responses. In summary, these therapies effectively control the inflammatory response in IBD and alleviate associated depressive symptoms through common mechanisms like immune regulation and inflammation suppression, thereby providing multiple effective strategies for comprehensively managing the psychological health of IBD patients.

The NLRP3 inflammasome is crucial in neuroinflammation mediated by microglial cell activation. Initially, the activated NLRP3 inflammasome triggers caspase-1, thus cleaving the precursor cytokines pro-IL-1β and pro-IL-18 into active IL-1β and IL-18. These cytokines are secreted extracellular via the secretory pathway, thereby advancing the inflammatory response.[42] In addition, caspase-1 cleaves Gasdermin D (GSDMD), whose N-terminal fragment

forms membrane pores for the leakage of cellular contents and pyroptosis. As a result, local inflammation is exacerbated, and more inflammatory mediators are released, which continuously secrete pro-inflammatory factors that stimulate microglial cells and keep them in an activated inflammatory state, thereby initiating and aggravating neuroinflammation.[43,44]

Noteworthy, the NLRP3 inflammasome activation is regulated by oxidative stress. Specifically, oxidative stress induces mitochondrial dysfunction, causing the release of danger signals like mitochondrial DNA and cardiolipin, which NLRP3 recognizes to activate the NLRP3 inflammasome.[45] Additionally, oxidative stress can induce the dissociation of thioredoxin-interacting protein (TXNIP) from thioredoxin, and TXNIP binds to NLRP3 to promote the assembly and activation of the NLRP3 inflammasome.[46] Oxidative stress may also cause the efflux of potassium ions, and the resultant low-potassium environment is crucial for NLRP3 inflammasome activation.[47] Excessive oxidative stress further enhances the NLRP3 inflammasome response through oxidative modification of NLRP3 and its accessory proteins. Ultimately, the interaction between ASC and Caspase-1 is promoted, Caspase-1 is activated, the maturation and secretion of pro-inflammatory cytokines IL-1β and IL-18 are accelerated, and pyroptosis is induced. In this process, changes in oxidative and antioxidative molecules like protein hydroxyl groups, 4-HNE, and GPx can effectively reflect the changes in the oxidative stress state. Through these mechanisms, oxidative stress regulates the activation of the NLRP3 inflammasome and the progression of neuroinflammation.

This research found that the DSS-induced IBD models displayed depressive-like behaviors, accompanied by notably increased relative protein expression levels of NLRP3, ASC, and Caspase-1 in the prefrontal cortex (PFC). Furthermore, significantly increased levels of inflammatory cytokines IL-1β, IL-6, and TNF-α were observed. Following electroacupuncture, the relative protein expression levels of NLRP3, ASC, and Caspase-1 in PFC decreased notably compared to the DSS group, the protein contents of IL-1β, IL-6, and TNF-α were significantly reduced, and depressive-like symptoms were evidently mitigated, demonstrated by a significant decrease in immobility time in the tail suspension and forced swim tests. These results were further validated based on NLRP3 inhibitor MCC950, which showed that the inhibitory effects of electroacupuncture on NLRP3 were comparable to those of MCC950. This further substantiates that the NLRP3/ASC/Caspase-1 signaling pathway is likely a key pathway through which electroacupuncture regulates abnormal microglial activation and alleviates neuroinflammation.

Additionally, the contents of protein hydroxyl groups and 4-HNE in the PFC of IBD mice were significantly reduced following electroacupuncture, whereas the antioxidant enzyme GPx showed a notable increase. Thus, electroacupuncture can effectively mitigate oxidative stress. Meanwhile, electroacupuncture significantly decreased the mRNA transcription levels of NLRP3, ASC, Caspase-1, and GSDMD. Therefore, electroacupuncture can effectively inhibit NLRP3 inflammasome activation. In conclusion, this research suggests that electroacupuncture may suppress microglial cell activation and ameliorate neuroinflammation by modulating the oxidative stress-mediated NLRP3/ASC/Caspase-1 signaling pathway. The mechanism schematic is given in Figure 7 summarized from the previous analysis.

Although this study elucidates how EA alleviates IBD-associated depression by modulating the oxidative stress-NLRP3/ASC/Caspase-1 pathway to suppress microglial activation, several limitations warrant attention. First, while the necessity of the NLRP3 pathway was pharmacologically confirmed using MCC950, direct genetic rescue experiments (eg, NLRP3 overexpression or knockout) are lacking to establish definitive causality. Future studies will employ brain-region-specific gene manipulations (eg, AAV-mediated) to validate target specificity. In addition, given the high prevalence of anxiety in IBD patients, incorporating anxiety-like behavioral tests (eg, elevated plus maze) in future study is crucial. Eventually, this study focuses primarily on the regulatory effects of electroacupuncture on the NLRP3/ASC/Caspase-1 signaling pathway, while whether the substances released during oxidative stress are key molecules regulating this pathway requires further verification. Addressing these gaps will advance the precision application of EA in IBD-related neuropsychiatric comorbidities.

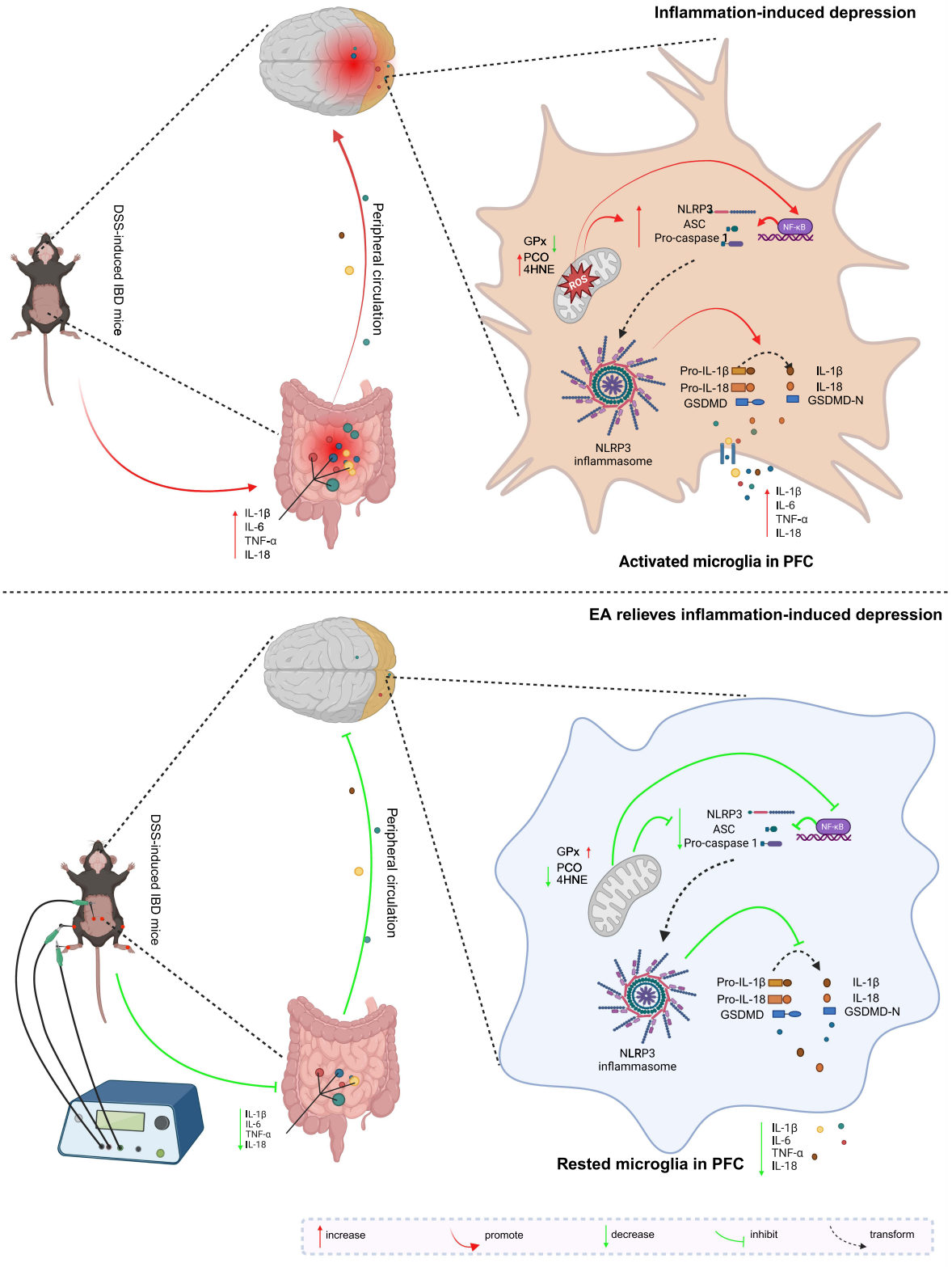

Figure 7 Mechanism of electroacupuncture in alleviating IBD-related depression through modulation of the NLRP3 inflammasome and neuroinflammation. *Created in BioRender. Zuqiang, (L) (2025) https://BioRender.com/b01p810.*

https://doi.org/10.2147/JIR.S534219

Conclusion

Overall, this study provides new insights into the treatment of depressive symptoms induced by ulcerative colitis. The results indicate that electroacupuncture exhibits an anti-depressive effect by improving oxidative stress in the PFC while reducing NLRP3 inflammasome recruitment, thereby inhibiting microglial cell over-activation and alleviating neuroinflammation. These findings provide important references for treating IBD complicated by depression through acupuncture.

Acknowledgments

We thank everyone who contributed to this research and contributed to the publication of this article.

Funding

This work was supported by The National Natural Science Foundation of China (Nos. 82474662, 81774438 AND 81904097), Natural Science Foundation of Hunan Province (No. 2023JJ30457), Natural Science Foundation of Changsha (No.kq2208183), Hunan Provincial Health High-Level Talent Scientific Research Project (No.R2023141), Scientific Research Project of Hunan Provincial Department of Education (No. 22C0198, No. 23A0284), Project of Chinese Medicine Research in Hunan Province (No. C2022027), The Science and Technology Innovation Program of Hunan Province (No. 2024JK2132, No. 2024RC1061), Projects of Administration of Traditional Chinese Medicine of Hunan Province (No.B2023109), the State Administration of Traditional Chinese Medicine 2022 Youth Qihuang Scholars Training Program (National Letter of Traditional Chinese Medicine Education [2022] 256) and the School-level Scientific Research Fund Project of Hunan University of Chinese Medicine School-level Scientific Research Fund Project (No. 2023CX167).

Disclosure

The author(s) report no conflicts of interest in this work.

References

1. Cho CW, You M-W, Oh CH, Lee CK, Moon SK. Long-term disease course of Crohn's disease: changes in disease location, phenotype, activities, and predictive factors. *Gut Liver*. 2022;16(2):157. doi:10.5009/gnl210118
2. Vuyyuru SK, Kedia S, Sahu P, Ahuja V. Immune-mediated inflammatory diseases of the gastrointestinal tract: beyond Crohn's disease and ulcerative colitis. *JGH Open*. 2022;6(2):100–111. doi:10.1002/jgh3.12706
3. Fairbrass KM, Gracie DJ, Ford AC. Healthy mind, healthy body: chronic depression may predate the development of inflammatory bowel disease by up to 9 years. *Gastroenterology*. 2021;160(7):2611–2613. doi:10.1053/j.gastro.2021.02.004
4. Piovani D, Armuzzi A, Bonovas S. Association of depression with incident inflammatory bowel diseases: a systematic review and meta-analysis. *Inflamm Bowel Dis*. 2024;30(4):573–584. doi:10.1093/ibd/izad109
5. Roberts C, Gamwell K, Edwards C, et al. P045 illness stigma, body image dissatisfaction, twarted belongingness, and depressive symptoms in youth with inflammatory bowel disease. *Gastroenterology*. 2020;158(3):S104. doi:10.1053/j.gastro.2019.11.246
6. Li P, Zheng J, Bai Y, et al. Characterization of kynurenine pathway in patients with diarrhea-predominant irritable bowel syndrome. *Eur J Histochem*. 2020;64(Suppl 2). doi:10.4081/ejh.2020.3132
7. Xie J, Liu L, Guo H, et al. Orally administered melanin from Sepiapharaonis ink ameliorates depression-anxiety-like behaviors in DSS-induced colitis by mediating inflammation pathway and regulating apoptosis. *Int Immunopharmacol*. 2022;106:108625. doi:10.1016/j.intimp.2022.108625
8. Wang H, He Y, Sun Z, et al. Microglia in depression: an overview of microglia in the pathogenesis and treatment of depression. *J Neuroinflammation*. 2022;19(1):132. doi:10.1186/s12974-022-02492-0
9. Varghese SM, Patel S, Nandan A, et al. Unraveling the role of the blood-brain barrier in the pathophysiology of depression: recent advances and future perspectives. *Mol Neurobiol*. 2024. doi:10.1007/s12035-024-04205-5
10. Olcum M, Tufekci KU, Durur DY, et al. Ethyl Pyruvate attenuates microglial NLRP3 inflammasome activation via inhibition of HMGB1/NF-κB/miR-223 signaling. *Antioxidants*. 2021;10(5):745. doi:10.3390/antiox10050745
11. Sun W, Wang Q, Zhang R, Zhang N. Ketogenic diet attenuates neuroinflammation and induces conversion of M1 microglia to M2 in an EAE model of multiple sclerosis by regulating the NF-κB/NLRP3 pathway and inhibiting HDAC3 and P2X7R activation. *Food Funct*. 2023;14(15):7247–7269. doi:10.1039/D3FO00122A
12. Han C, Pei H, Shen H, et al. Antcin K targets NLRP3 to suppress neuroinflammation and improve the neurological behaviors of mice with depression. *Int Immunopharmacol*. 2023;117:109908. doi:10.1016/j.intimp.2023.109908
13. Zhao T, Piao L-H, Li D-P, et al. BDNF gene hydroxymethylation in hippocampus related to neuroinflammation-induced depression-like behaviors in mice. *J Affective Disorders*. 2023;323:723–730. doi:10.1016/j.jad.2022.12.035
14. Cheon SY, Kim M-Y, Kim J, et al. Hyperammonemia induces microglial NLRP3 inflammasome activation via mitochondrial oxidative stress in hepatic encephalopathy. *Biomedical Journal*. 2023;46(5):100593. doi:10.1016/j.bj.2023.04.001

15. Long M, Wang Z, Zheng D, et al. Electroacupuncture pretreatment elicits neuroprotection against cerebral ischemia-reperfusion injury in rats associated with transient receptor potential vanilloid 1-mediated anti-oxidant stress and anti-inflammation. *Inflammation*. 2019;42:1777–1787. doi:10.1007/s10753-019-01040-y
16. Bao C, Zhang J, Wu H. Acupuncture for Crohn's disease: Current status and future perspectives. *Acupunct Herb Med*. 2023;3(4):229–231. doi:10.1097/HM9.0000000000000081
17. Yin X, Li W, Liang T, et al. Effect of electroacupuncture on insomnia in patients with depression: a randomized clinical trial. *JAMA Network Open*. 2022;5(7):e2220563–e2220563. doi:10.1001/jamanetworkopen.2022.20563
18. Li M, Yang F, Zhang X, et al. Electroacupuncture attenuates depressive-like behaviors in poststroke depression mice through promoting hippocampal neurogenesis and inhibiting TLR4/NF-κB/NLRP3 signaling pathway. *NeuroReport*. 2024;35(14):947–960. doi:10.1097/WNR.0000000000002088
19. Pang F, Yang Y, Huang S, et al. Electroacupuncture alleviates depressive-like behavior by modulating the expression of P2X7/NLRP3/IL-1β of prefrontal cortex and liver in rats exposed to chronic unpredictable mild stress. *Brain Sciences*. 2023;13(3):436. doi:10.3390/brainsci13030436
20. Chen Q, Fang Z, Yang Z, et al. Lactobacillus plantarum-derived extracellular vesicles modulate macrophage polarization and gut homeostasis for alleviating ulcerative colitis. *J Agric Food Chem*. 2024;72:14713–14726.
21. Bauer C, Duewell P, Mayer C, et al. Colitis induced in mice with dextran sulfate sodium (DSS) is mediated by the NLRP3 inflammasome. *Gut*. 2010;59(9):1192–1199. doi:10.1136/gut.2009.197822
22. Gao R, Ren Y, Xue P, et al. Protective effect of the polyphenol ligustroside on colitis induced with dextran sulfate sodium in mice. *Nutrients*. 2024;16(4). doi:10.3390/nu16040522
23. Wirtz S, Popp V, Kindermann M, et al. Chemically induced mouse models of acute and chronic intestinal inflammation. *Nat Protoc*. 2017;12 (7):1295–1309. doi:10.1038/nprot.2017.044
24. Bisgaard TH, Allin KH, Elmahdi R, Jess T. The bidirectional risk of inflammatory bowel disease and anxiety or depression: a systematic review and meta-analysis. *Gen Hospital Psychiatr*. 2023;83:109–116. doi:10.1016/j.genhosppsych.2023.05.002
25. Craig CF, Filippone RT, Stavely R, Bornstein JC, Apostolopoulos V, Nurgali K. Neuroinflammation as an etiological trigger for depression comorbid with inflammatory bowel disease. *J Neuroinflammation*. 2022;19(1):4.
26. Stolzer I, Scherer E, Süß P, et al. Impact of microbiome–brain communication on neuroinflammation and neurodegeneration. *Int J Mol Sci*. 2023;24 (19):14925. doi:10.3390/ijms241914925
27. Sun Y, Koyama Y, Shimada S. Inflammation from peripheral organs to the brain: how does systemic inflammation cause neuroinflammation? *Front Aging Neurosci*. 2022;14:903455. doi:10.3389/fnagi.2022.903455
28. Fujita Y, Yamashita T. Neuroprotective function of microglia in the developing brain. *Neuronal Signal*. 2021;5(1):NS20200024. doi:10.1042/NS20200024
29. Lukens JR, Eyo UB. Microglia and neurodevelopmental disorders. *Ann Rev Neurosci*. 2022;45(1):425–445. doi:10.1146/annurev-neuro-110920-023056
30. Fang S, Wu Z, Guo Y, et al. Roles of microglia in adult hippocampal neurogenesis in depression and their therapeutics. *Front Immunol*. 2023;14:1193053. doi:10.3389/fimmu.2023.1193053
31. Li C, Liu B, Xu J, et al. Phloretin decreases microglia-mediated synaptic engulfment to prevent chronic mild stress-induced depression-like behaviors in the mPFC. *Theranostics*. 2023;13(3):955. doi:10.7150/thno.76553
32. Cao P, Chen C, Liu A, et al. Early-life inflammation promotes depressive symptoms in adolescence via microglial engulfment of dendritic spines. *Neuron*. 2021;109(16):2573–2589.e9. doi:10.1016/j.neuron.2021.06.012
33. Duan N, Zhang Y, Tan S, et al. Therapeutic targeting of STING-TBK1-IRF3 signalling ameliorates chronic stress induced depression-like behaviours by modulating neuroinflammation and microglia phagocytosis. *Neurobiol Dis*. 2022;169:105739. doi:10.1016/j.nbd.2022.105739
34. Fan C, Li Y, Lan T, Wang W, Long Y, Yu SY. Microglia secrete miR-146a-5p-containing exosomes to regulate neurogenesis in depression. *Mol Ther*. 2022;30(3):1300–1314. doi:10.1016/j.ymthe.2021.11.006
35. Xu X, Piao HN, Aosai F, et al. Arctigenin protects against depression by inhibiting microglial activation and neuroinflammation via HMGB1/TLR4/NF-κB and TNF-α/TNFR1/NF-κB pathways. *Br J Pharmacol*. 2020;177(22):5224–5245. doi:10.1111/bph.15261
36. Zhou S, Huang Z, Hou W, Lin Y, Yu J. Prospective study of an Adalimumab combined with partial enteral nutrition in the induction period of Crohn's disease. *Inflammation Res*. 2024;73(2):199–209. doi:10.1007/s00011-023-01828-7
37. Lee YN, Mansur RB, Brietzke E, et al. Efficacy of adjunctive infliximab vs. placebo in the treatment of anhedonia in bipolar I/II depression. *Brain Behav Immun*. 2020;88:631–639. doi:10.1016/j.bbi.2020.04.063
38. Onisor D, Avram C, Ruta F, et al. Burden of common mental disorders in ulcerative colitis and irritable bowel syndrome patients: an analysis of risk factors. *J Clin Med*. 2025;14(2):499. doi:10.3390/jcm14020499
39. Long MD, Afzali A, Fischer M, et al. Tofacitinib response in ulcerative colitis (TOUR): early response after initiation of tofacitinib therapy in a real-world setting. *Inflamm Bowel Dis*. 2023;29(4):570–578. doi:10.1093/ibd/izac121
40. Yoo J-W, Shin Y-J, Ma X, et al. The alleviation of gut microbiota-induced depression and colitis in mice by anti-inflammatory probiotics NK151, NK173, and NK175. *Nutrients*. 2022;14(10):2080. doi:10.3390/nu14102080
41. Zhao H, Chen X, Zhang L, et al. Ingestion of Lacticaseibacillus Rhamnosus Fmb14 prevents depression-like behavior and brain neural activity via the microbiota–gut–brain axis in colitis mice. *Food Funct*. 2023;14(4):1909–1928. doi:10.1039/D2FO04014J
42. Han Q, Li W, Chen P, et al. Microglial NLRP3 inflammasome-mediated neuroinflammation and therapeutic strategies in depression. *Neural Regen Res*. 2024;19(9):1890–1898. doi:10.4103/1673-5374.390964
43. Su L, Lu H, Zhang D, et al. Total paeony glycoside relieves neuroinflammation to exert antidepressant effect via the interplay between NLRP3 inflammasome, pyroptosis and autophagy. *Phytomedicine*. 2024;128:155519. doi:10.1016/j.phymed.2024.155519
44. Zhang Z, Chen H, Han L, Liu K, Du S, Gao R. Inhibition of the NLRP3/caspase-1 cascade related pyroptosis relieved propofol-induced neuroinflammation and cognitive impairment in developing rats. *Free Radic Biol Med*. 2024;225:87–97. doi:10.1016/j.freeradbiomed.2024.09.038
45. Luo G, Chen L, Chen M, et al. Hirudin inhibit the formation of NLRP3 inflammasome in cardiomyocytes via suppressing oxidative stress and activating mitophagy. *Heliyon*. 2024;10(1).
46. Zhang W, Yu W, Zhu Y, Gu J, Gu X. Alda-1 ameliorates oxidative stress-induced cardiomyocyte damage by inhibiting the mitochondrial ROS/TXNIP/NLRP3 pathway. *J Biochem Mol Toxicol*. 2024;38(11):e70032. doi:10.1002/jbt.70032
47. Wang L, Negro R, Wu H. TRPM2, linking oxidative stress and Ca2+ permeation to NLRP3 inflammasome activation. *Curr Opin Immunol*. 2020;62:131–135. doi:10.1016/j.coi.2020.01.005